Supporting Information

Synergistic CoN-Decorated Pt Catalyst on Two-Dimensional Porous Co-N-Doped Carbon Nanosheet for Enhanced Oxygen Reduction Activity and Durability

*Thanh-Nhan Tran, [#] Ha-Young Lee, [#] Jong-Doek Park, Tong-Hyun Kang, Byong-June Lee, and Jong-Sung Yu**

Email: jsyu@dgist.ac.kr

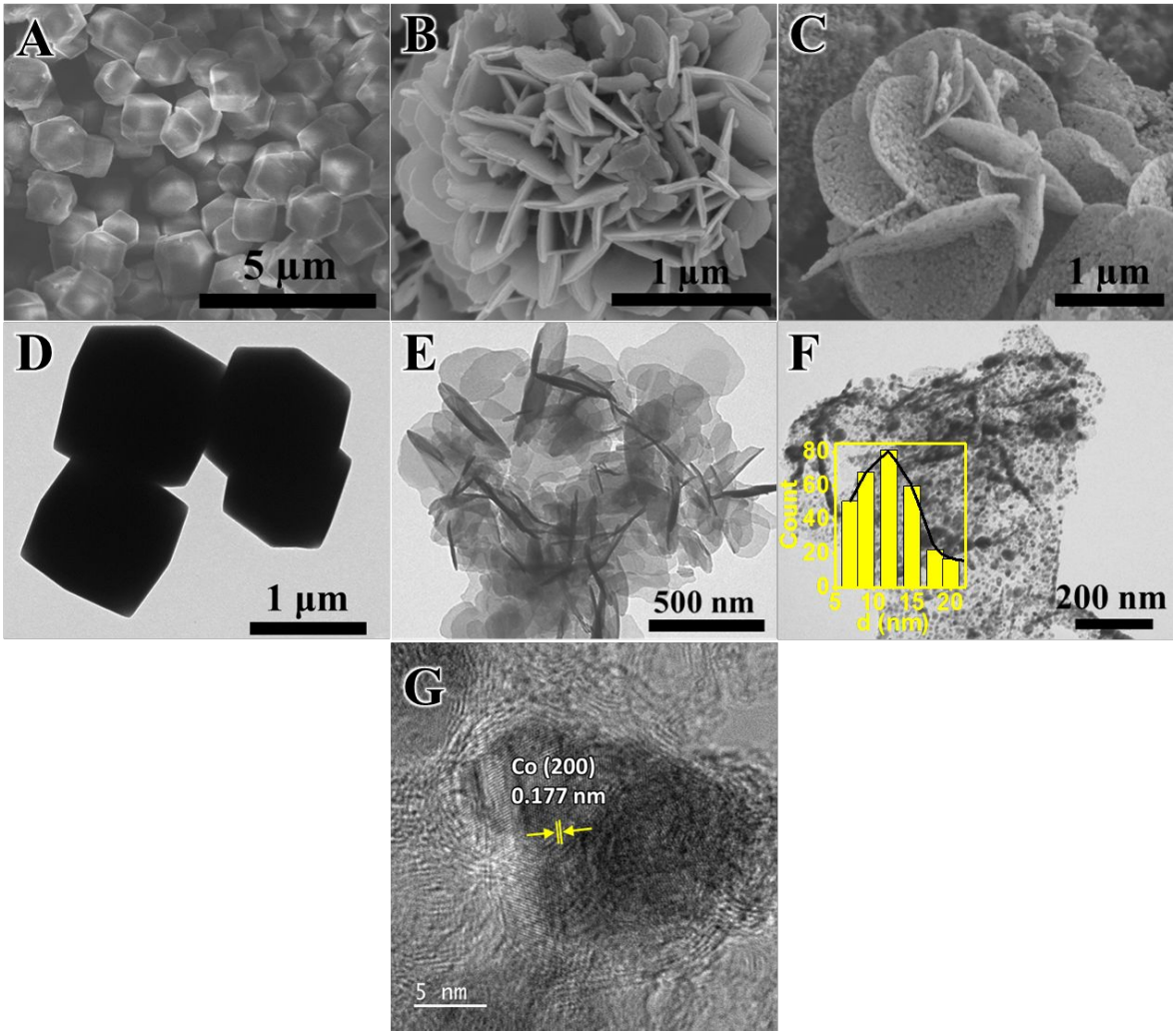

Figure S1. (A-C) SEM and (D-F) TEM images of as-prepared ZIF-67, NF-CoZIF and Co/CoNC-2D, respectively, and (G) HR-TEM image of Co/CoNC-2D along with Co lattice spacing.

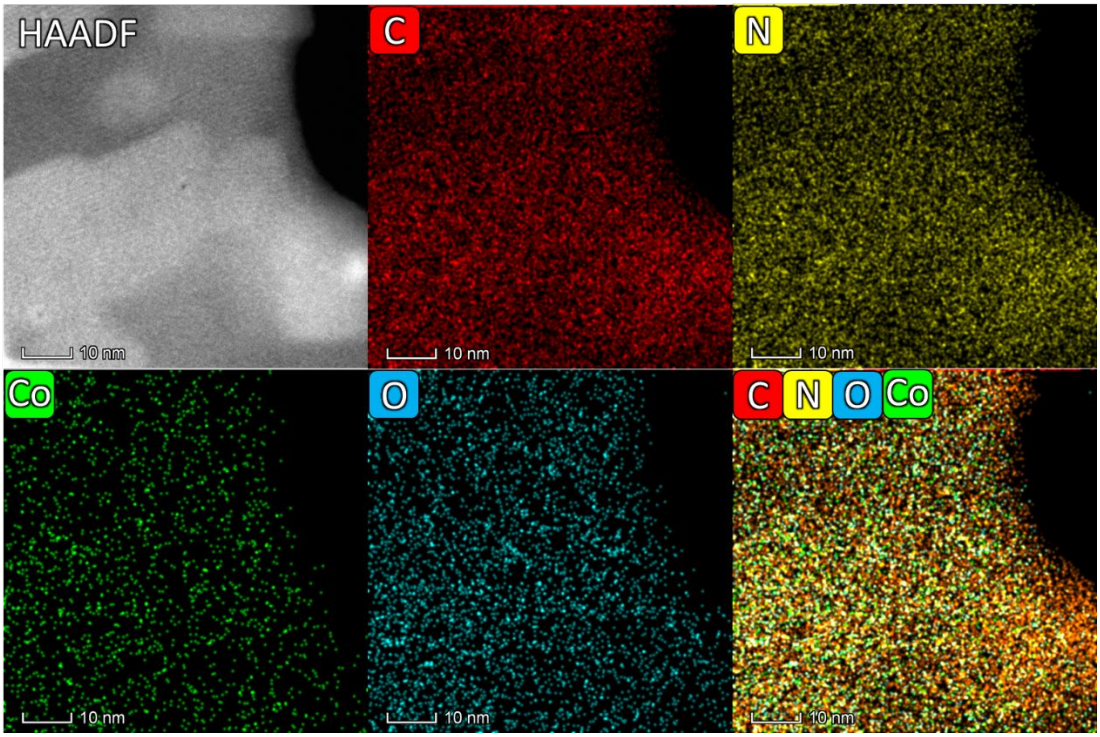

Figure S2. HAADF-STEM image of NF-CoZIF and EDS elemental mapping images for C, N, Co and O, and the merged image, respectively.

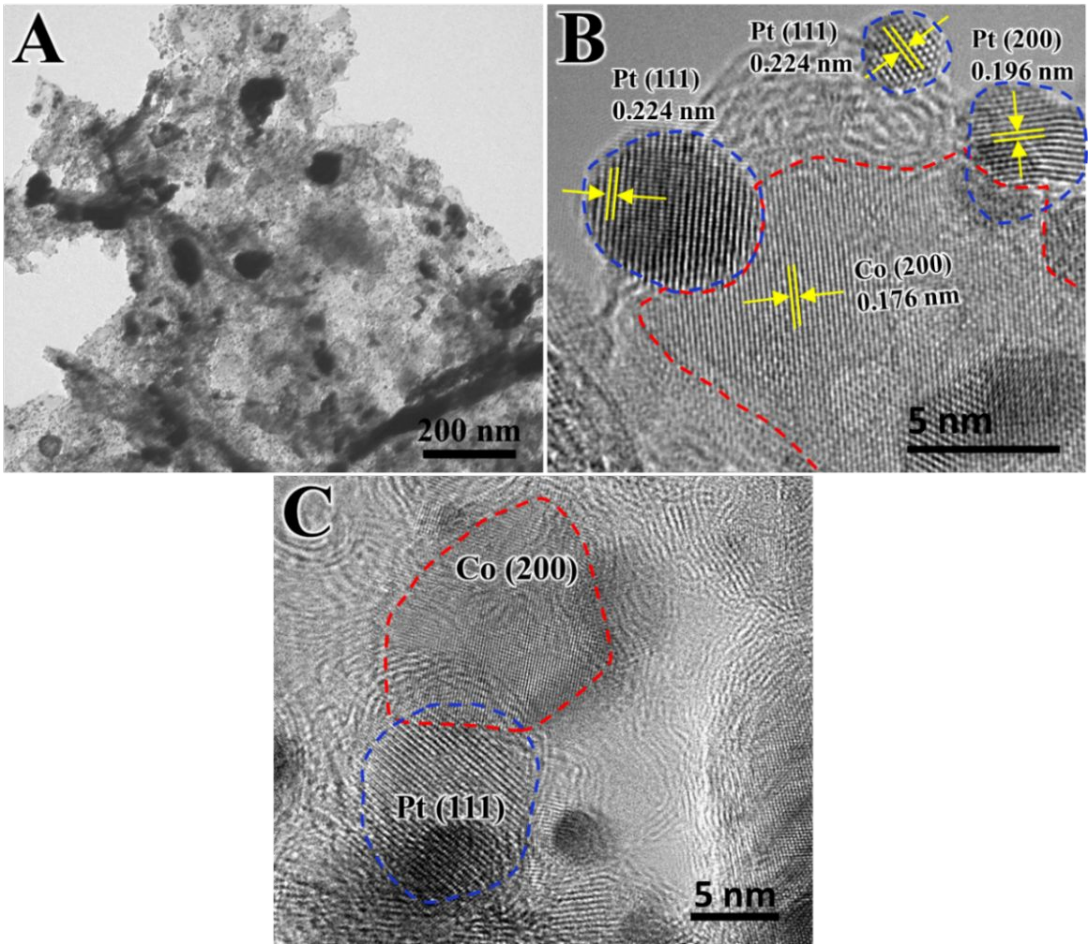

Figure S3. (A) TEM and (B, C) HR-TEM images for crystallite lattices of PtCo/CoNC-2D.

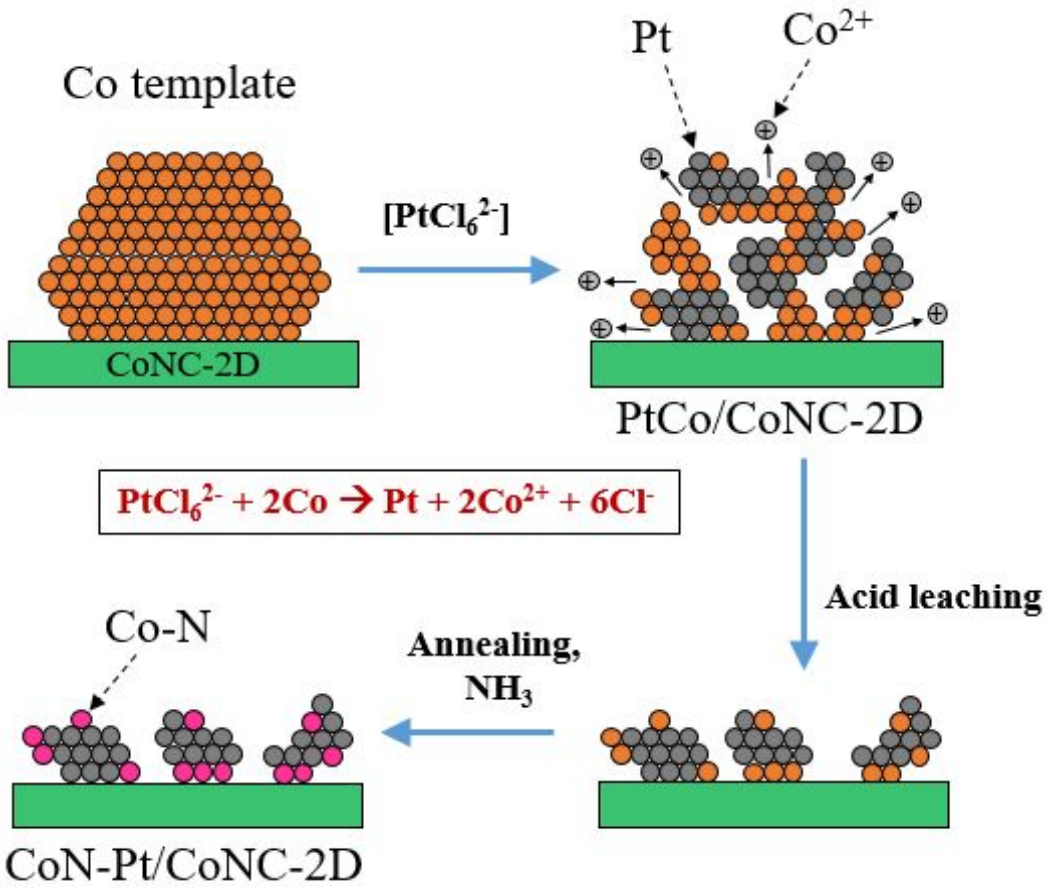

Figure S4. Schematic representation of Pt NPs growth pathway by galvanic replacement reaction on Co template. The undissolved Co traces on Pt surface are convented to CoN after NH_3 heat treatment to generate CoN-Pt/CoNC-2D.

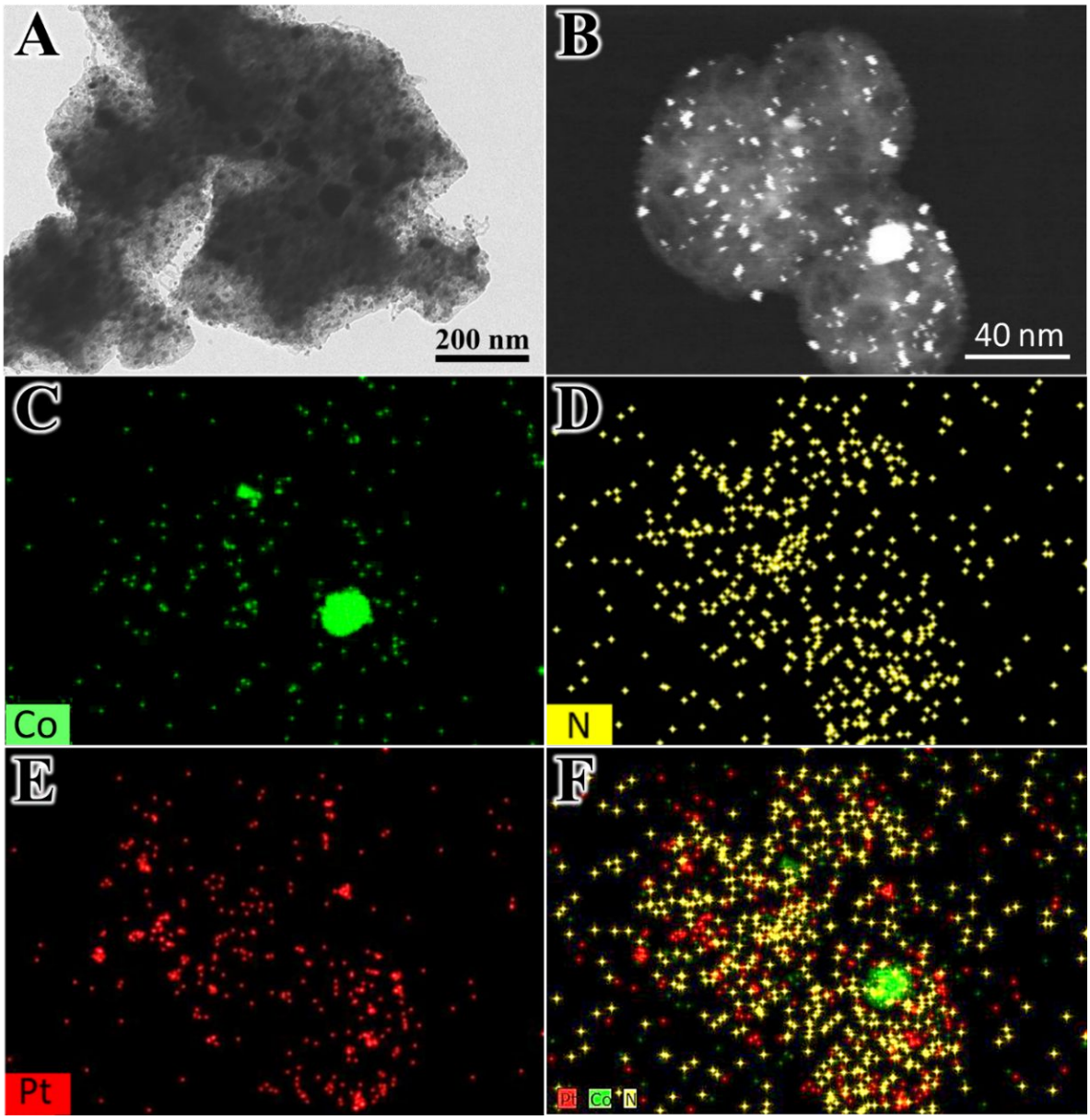

Figure S5. (A) TEM, (B) HAADF-STEM images of CoN-Pt/CoNC-bulk and (C-F) EDS elemental mapping images for Co, N and Pt, and the merged image, respectively.

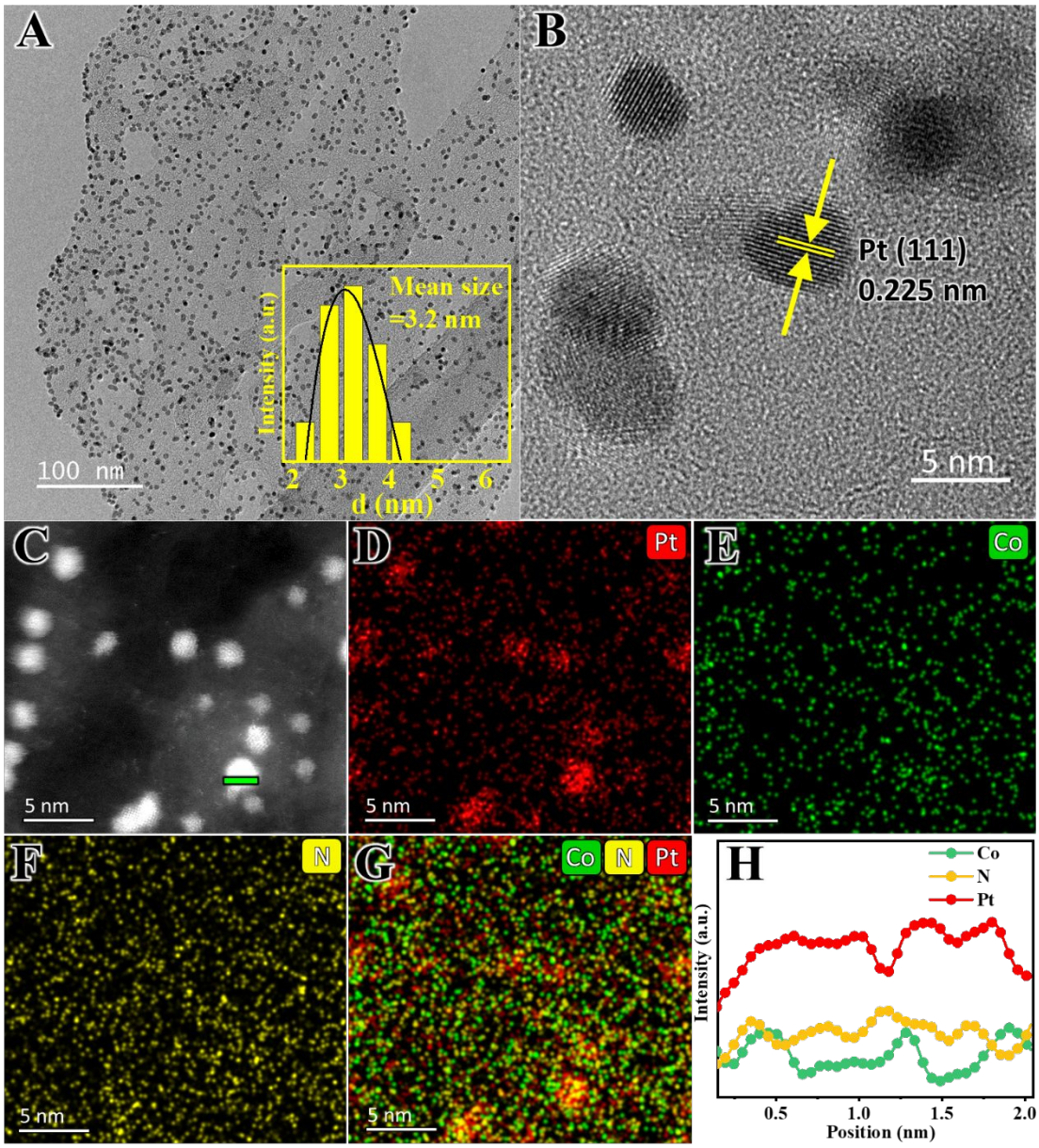

Figure S6. (A) TEM, (B) HR-TEM, (C) HAADF-STEM images of Pt/CoNC-2D and (D-G) EDS elemental mapping images for Pt, Co, N and the merged image, respectively. (H) Resulting element line profiles of a green line in image C with Pt, Co and N element signal intensity.

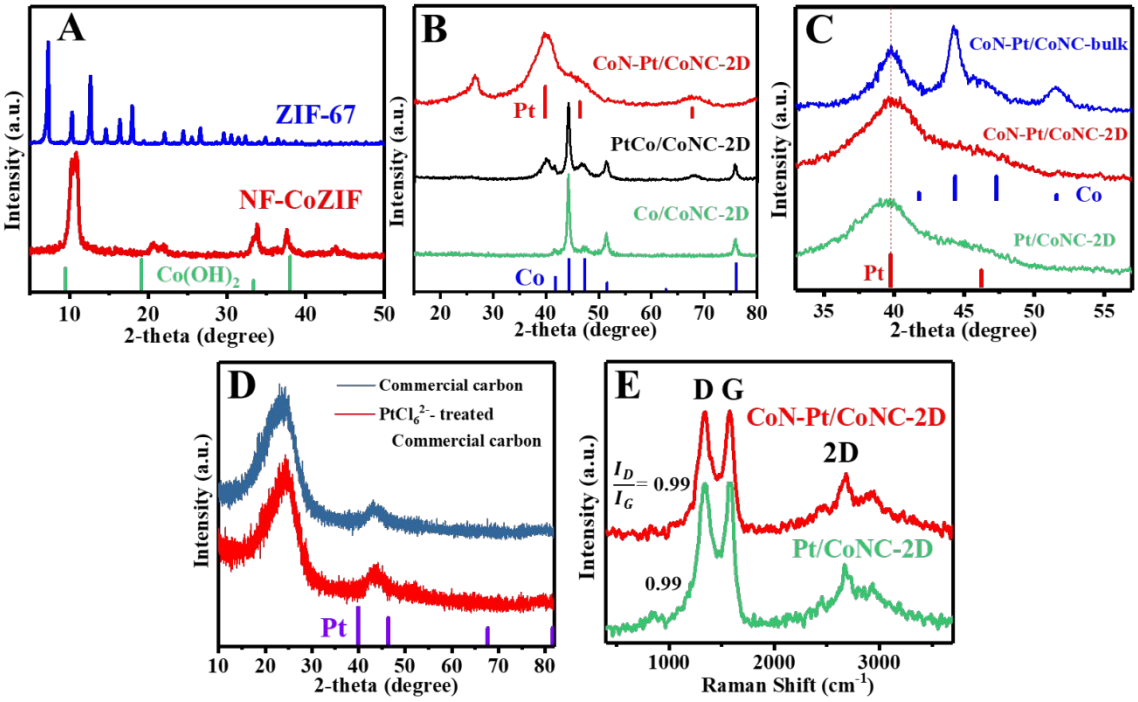

Figure S7. XRD patterns of (A) ZIF-67 and NF-CoZIF, (B) Co/CoNC-2D, PtCo/CoNC-2D, and CoN-Pt/CoNC-2D, (C) Pt/CoNC-2D, CoN-Pt/CoNC-2D, and CoN-Pt/CoNC-bulk and (D) commercial carbon before and after adding $PtCl_6^{2-}$ into the carbon in EG at 80 °C for 4 h. (E) Raman spectra of Pt/CoNC-2D and CoN-Pt/CoNC-2D.

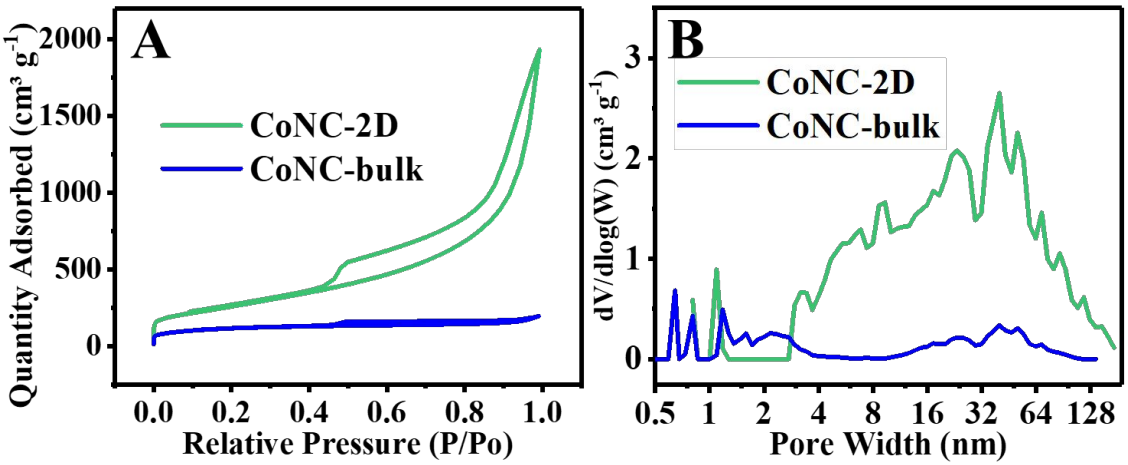

Figure S8. (A) nitrogen adsorption-desorption isotherms and (B) pore size distribution of CoNC-2D and CoNC-bulk samples.

Table S1. Physicochemical properties of as-prepared CoN-Pt/CoNC-2D, CoN-Pt/CoNC-bulk, CoNC-2D and CoNC-bulk samples.

Samples	S_{BET} (m^2 g^{-1})	S_{micro} (m^2 g^{-1})	S_{mico}/S_{BET}	V (cm^3 g^{-1})
CoN-Pt/CoNC-2D	288	54	18.8%	1.21
CoN-Pt/CoNC-bulk	202	164	80.9%	0.25
CoNC-2D	960	184	19.2%	3.00
CoNC-bulk	426	344	80.7%	0.30

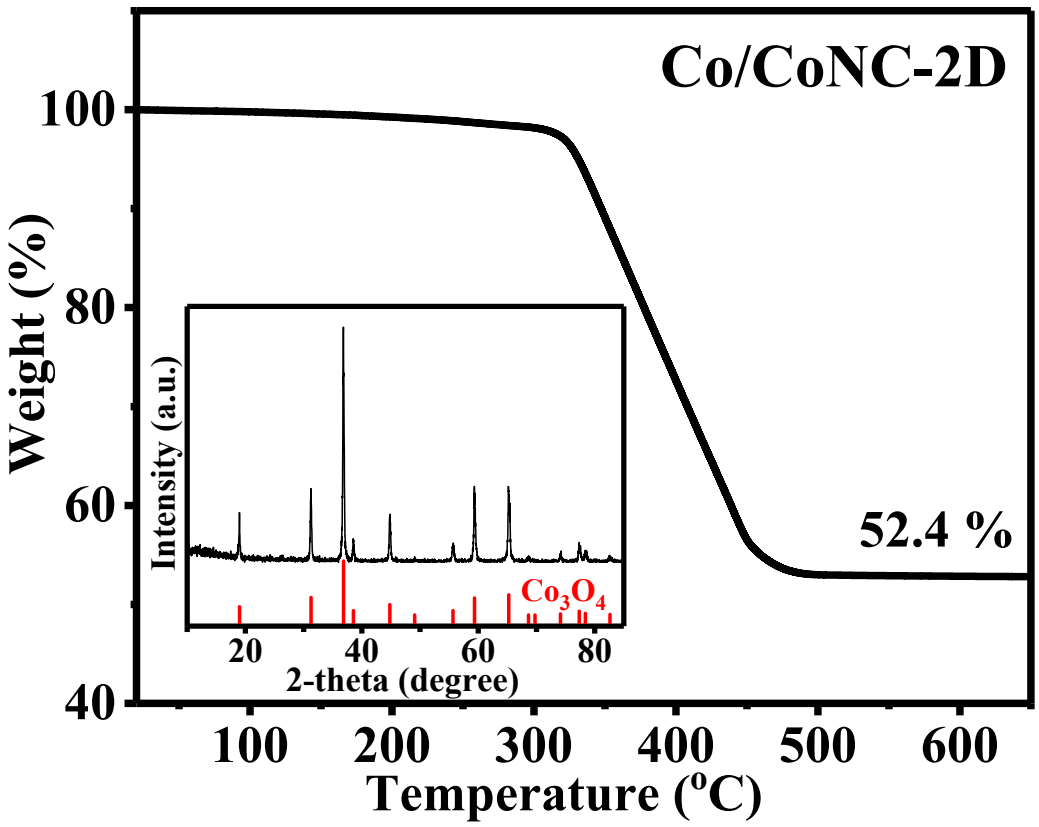

Figure S9. TGA plot of Co/CoNC-2D in air condition with a ramp of 5 °C min^{-1}. The inset shows XRD patterns of the Co/CoNC-2D residue after the TGA and Co_3O_4 reference (ICDD 00-043-1003).

Table S2. ICP results of all the as-prepared samples.

Material	ρ_{Pt} (μg/mL)	ρ_{Co} (μg/mL)	C_{Pt} (μmol/mL)	C_{Co} (μmol/mL)	Pt (wt%) in the sample	Co (wt%) in the sample
CoN-Pt/CoNC-2D	29.61	3.77	0.15	0.06	23.68	3.02
CoN-Pt/CoNC-bulk	26.19	15.47	0.13	0.26	20.95	12.38
Pt/CoNC-2D	30.10	2.51	0.15	0.04	24.08	2.01
PtCo/CoNC-2D	28.03	34.22	0.14	0.57	22.43	27.38
Co/CoNC-2D		49.10		0.83		39.28
CoNC-2D		2.91		0.05		2.32

Table S3. Atomic composition obtained from XPS spectra for as-prepared Pt/CoNC-2D, CoN-Pt/CoNC-bulk and CoN-Pt/CoNC-2D samples.

Samples	**C 1s (at%)**	**Pt 4f (at%/wt%)**	**Co 2p (at%/ wt%)**	**N 1s (at%)**	**O 1s (at%)**
CoN-Pt/CoNC-2D	87.98	2.06/**24.50**	0.65/2.34	4.77	4.54
CoN-Pt/CoNC-bulk	86.52	1.88/**21.36**	2.26/7.75	3.61	5.73
Pt/CoNC-2D	88.31	2.13/**25.32**	0.32/1.14	3.30	5.94

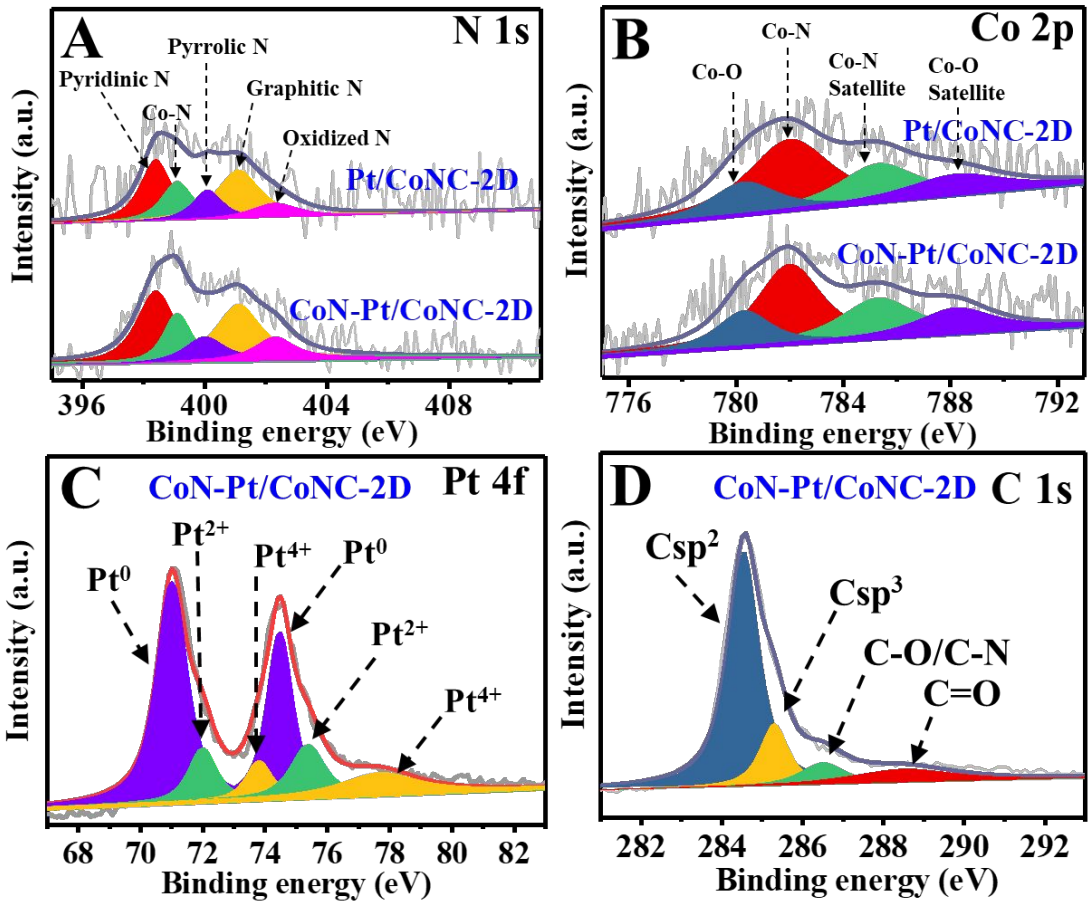

Figure S10. High resolution XPS spectra of (A) N 1s, (B) Co 2p of Pt/CoNC-2D and CoN-Pt/CoNC-2D, and typical deconvoluted (C) Pt 4f and (D) C 1s XPS spectra of CoN-Pt/CoNC-2D.

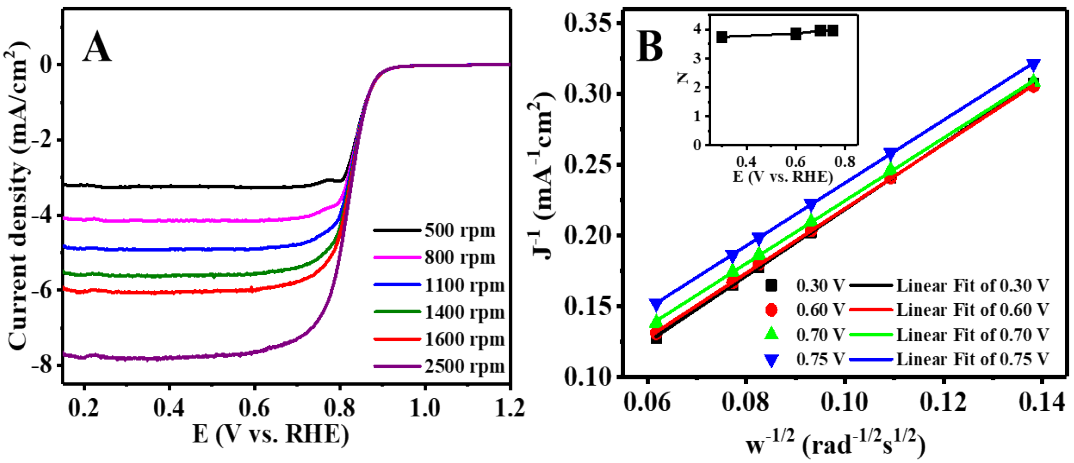

Figure S11. (A) LSV curves for different rotating speeds at 10 mV/s scan rate, (B) Koutecky-Levich plots at various potentials for the PtCo/CoNC-2D with inset for electron transferr number determined at various potentials.

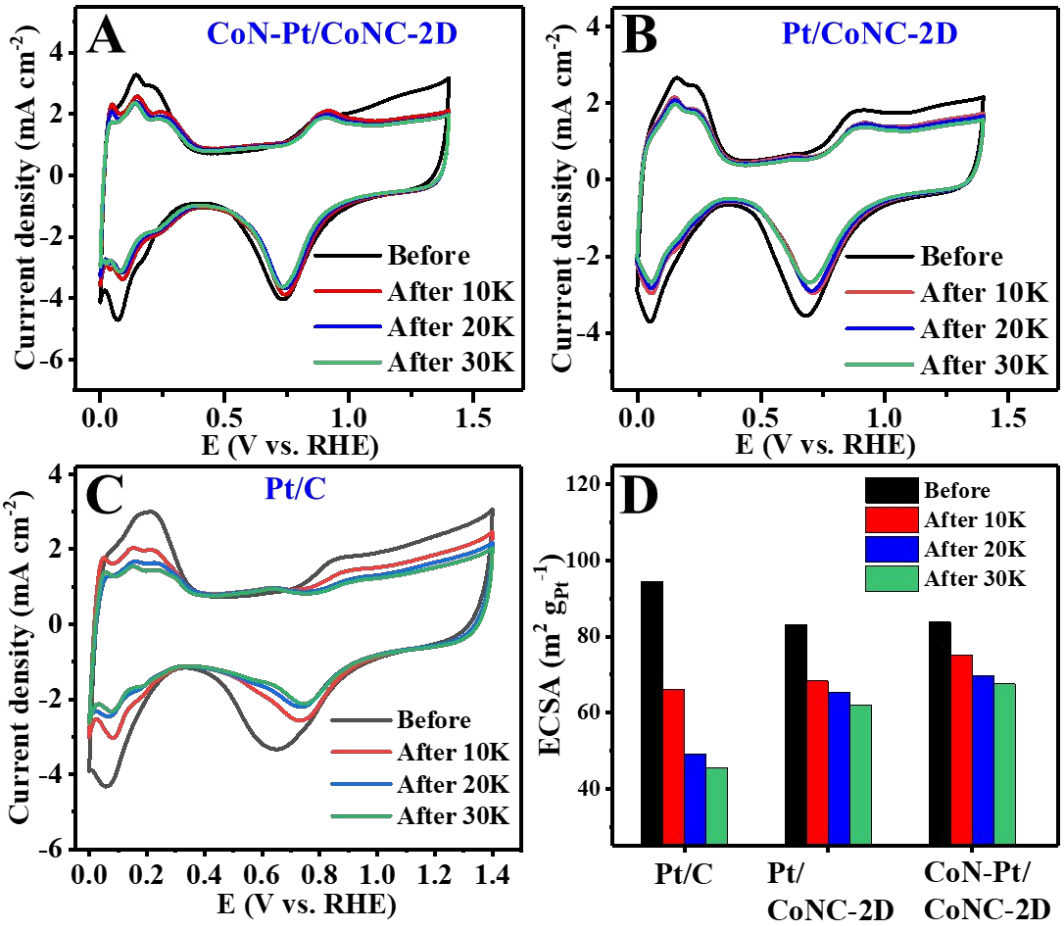

Figure S12. Full CV curves in N_2-saturated 0.1 M $HClO_4$ during ADT of (A) CoN-Pt/CoNC-2D, (B) Pt/CoNC-2D and (C) commercial Pt/C (20 wt%), and (D) changes in their ECSA during ADT.

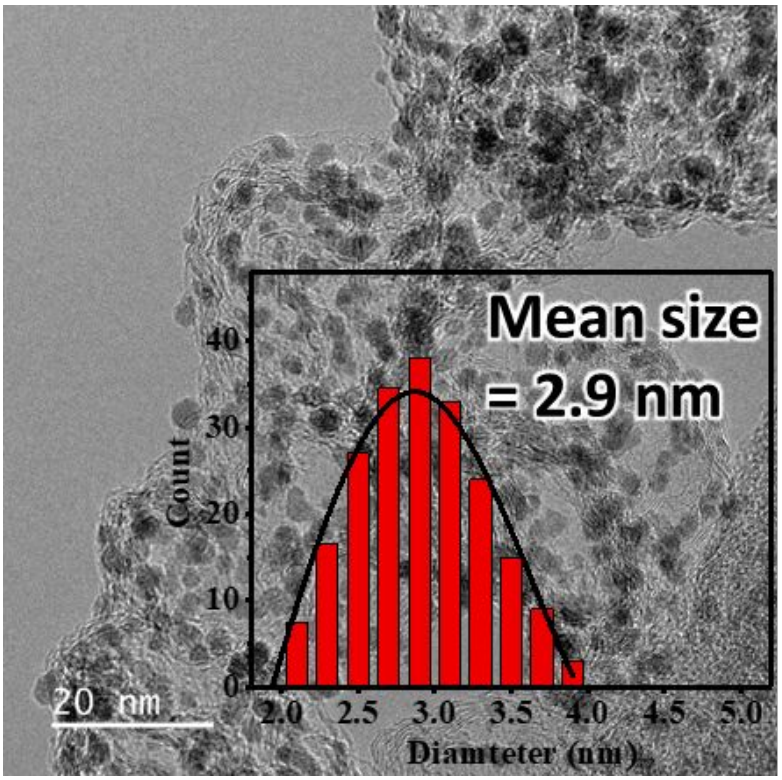

Figure S13. A typical TEM image of commercial Pt/C (20 wt%) before ADT.

Table S4. Comparison of the onset (E_{onset}), half-wave potential ($E_{1/2}$) and long-term durability for ORR of related PtCo/C catalysts from literature and this work.

Catalyst	E_{onset} relative to Pt/C	$E_{1/2}$ relative to Pt/C	Durability	Ref.
Pt_3Co/C	Similar	Positive shift ~ 50 mV	68% ECSA retention after 4000 cycles	1
Pt-Co/C	Similar	Positive shift ~ 17 mV	76% ECSA retention after 5000 cycles	2
PtCo/Co@NH PCC	Positive shift ~ 10 mV	Positive shift ~ 19 mV	70% ECSA retention after 5000 cycles	3
Pt_3Co/C-700	Positive shift ~ 40 mV	Positive shift ~ 70 mV	70% ECSA retention after 5000 cycles	4
PtCoNW	Positive shift ~ 20 mV	Positive shift ~ 40 mV	75% ECSA retention after 1000 cycles	5
Dendritic PtCo	Similar	Positive shift ~ 49 mV	NA	6
$Pt_{73}Co_{27}/C$	Similar	Positive shift ~ 20 mV	NA	7
CoN-Pt/CoNC-2D	**Similar**	**Positive shift ~ 50 mV**	80.6 % ECSA retention after 30000 cycles	**This Work**

Table S5. The electrochemical results of $E_{1/2}$, electrochemical surface area (ECSA), specific activity (SA), mass activity (MA), and Tafel slope measured by half-cell for CoN-Pt/CoNC-2D and Pt/CoNC2D and Pt/C in O_2-saturated 0.1 M $HClO_4$.

Sample	$E_{1/2}$ (V)	ECSA (m^2/g_{Pt})	SA (0.8V) (mA/cm^2_{Pt})	MA (0.8V) (mA/mg_{Pt})	Tafel slope (mV/dec)
CoN-Pt/CoNC-2D	0.83	83.8	0.059	49.72	49.5
Pt/CoNC-2D	0.81	83.1	0.045	37.06	65.8
Pt/C	0.78	94.5	0.033	31.25	89.9

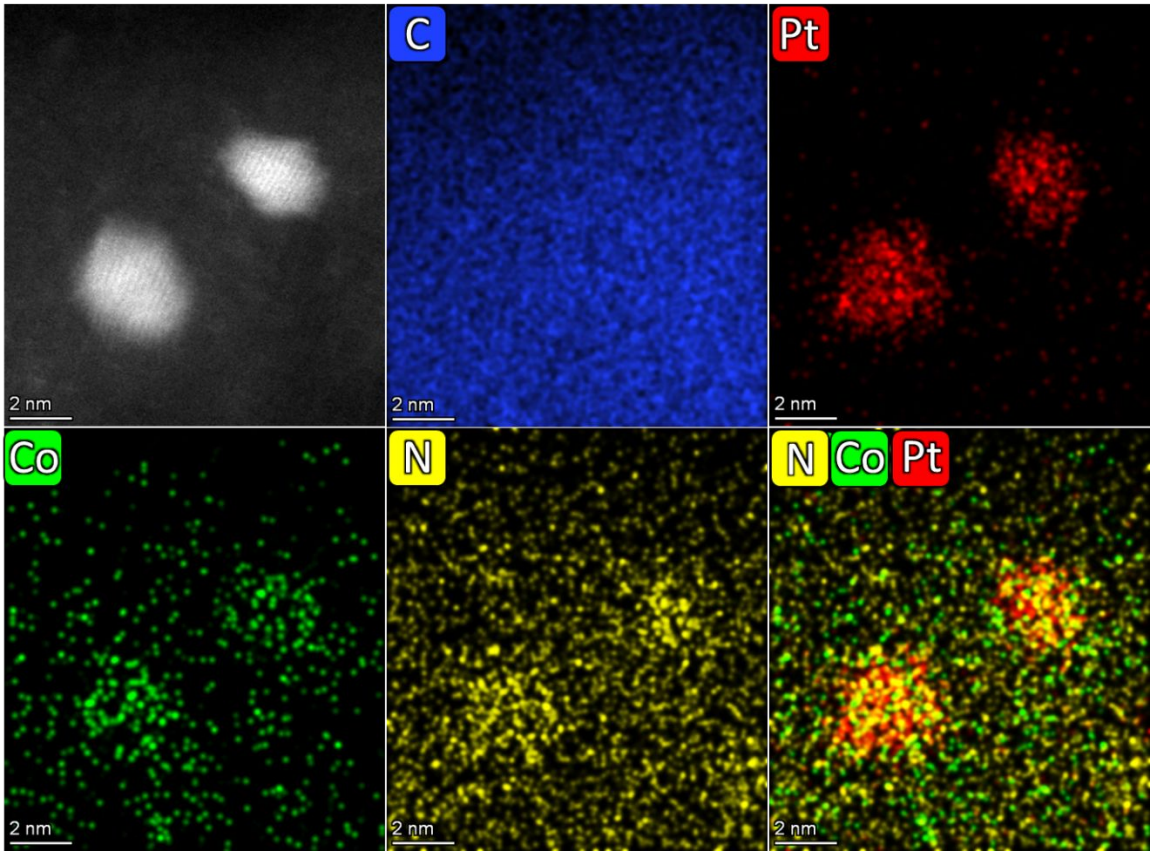

Figure S14. HAADF-STEM and EDS mapping images for C, Pt, Co, N, and the merged image of CoN-Pt/CoNC-2D after 30,000 potential cycles.

REFERENCES

(1) Lee, J. D.; Jishkariani, D.; Zhao, Y.; Najmr, S.; Rosen, D.; Kikkawa, J. M.; Stach, E. A.; Murray, C. B. Tuning the Electrocatalytic Oxygen Reduction Reaction Activity of Pt–Co Nanocrystals by Cobalt Concentration with Atomic-Scale Understanding. *ACS Appl. Mater. Interfaces* **2019**, *11* (30), 26789–26797. https://doi.org/10.1021/acsami.9b06346.

(2) Ma, Y.; Yin, L.; Yang, T.; Huang, Q.; He, M.; Zhao, H.; Zhang, D.; Wang, M.; Tong, Z. One-Pot Synthesis of Concave Platinum–Cobalt Nanocrystals and Their Superior Catalytic Performances for Methanol Electrochemical Oxidation and Oxygen Electrochemical Reduction. *ACS Appl. Mater. Interfaces* **2017**, *9* (41), 36164–36172. https://doi.org/10.1021/acsami.7b10209.

(3) Ying, J.; Li, J.; Jiang, G.; Cano, Z. P.; Ma, Z.; Zhong, C.; Su, D.; Chen, Z. Metal-Organic Frameworks Derived Platinum-Cobalt Bimetallic Nanoparticles in Nitrogen-Doped Hollow Porous Carbon Capsules as a Highly Active and Durable Catalyst for Oxygen Reduction Reaction. *Appl. Catal. B Environ.* **2018**, *225*, 496–503. https://doi.org/10.1016/j.apcatb.2017.11.077.

(4) Wang, D.; Xin, H. L.; Hovden, R.; Wang, H.; Yu, Y.; Muller, D. A.; Disalvo, F. J.; Abruña, H. D. Structurally Ordered Intermetallic Platinum-Cobalt Core-Shell Nanoparticles with Enhanced Activity and Stability as Oxygen Reduction Electrocatalysts. *Nat. Mater.* **2013**, *12* (1), 81–87. https://doi.org/10.1038/nmat3458.

(5) Higgins, D. C.; Wang, R.; Hoque, M. A.; Zamani, P.; Abureden, S.; Chen, Z. Morphology and Composition Controlled Platinum–Cobalt Alloy Nanowires Prepared by Electrospinning as Oxygen Reduction Catalyst. *Nano Energy* **2014**, *10*, 135–143. https://doi.org/10.1016/j.nanoen.2014.09.013.

(6) Wang, H.; Yuan, X.; Li, D.; Gu, X. Dendritic PtCo Alloy Nanoparticles as High Performance Oxygen Reduction Catalysts. *J. Colloid Interface Sci.* **2012**, *384* (1), 105–109. https://doi.org/10.1016/j.jcis.2012.06.060.

(7) Loukrakpam, R.; Shan, S.; Petkov, V.; Yang, L.; Luo, J.; Zhong, C. J. Atomic Ordering Enhanced Electrocatalytic Activity of Nanoalloys for Oxygen Reduction Reaction. *J. Phys. Chem. C* **2013**, *117* (40), 20715–20721. https://doi.org/10.1021/jp4067444.